Journal of Materials Chemistry A

ROYAL SOCIETY OF CHEMISTRY

PAPER

View Article Online
View Journal | View Issue

Cite this: J. Mater. Chem. A, 2020, 8, 18007

Strain-based chemical sensing using metal–organic framework nanoparticles†

H. H.-M. Yeung, ‡*[ab] G. Yoshikawa, [cd] K. Minami [bc] and K. Shiba *[bce]

Metal–organic frameworks (MOFs) have received much attention for their potential as chemical sensors, owing to unparalleled tunability of their host–guest response, high uptake and structural flexibility. However, because of the limited compatibility between MOF properties and sensor transduction mechanisms, very few MOFs have successfully been integrated into practical devices. We report the fabrication of the first strain-based sensor constructed from MOF nanoparticles deposited directly onto a membrane-type surface stress sensor (MSS) architecture, which exhibits unprecedented response times on the order of seconds and ppm-level sensitivity towards volatile organic compounds (VOCs). Finite element analysis is used to demonstrate that the sensor response is a result of analyte-induced strain in the MOF receptor layer. We show that an array of four types of MOF nanoparticles allows for clear discrimination between different classes of VOCs and even individual gases, using principal component analysis of their response profiles. This work opens up the possibility of VOC sensing using a wide range of MOFs, beyond those that are electrically conducting or those that form oriented thin films, with the added advantages of high sensitivity and rapid response compared to existing MOF strain-based sensors.

Received 24th July 2020
Accepted 6th August 2020

DOI: 10.1039/d0ta07248f

rsc.li/materials-a

Introduction

Sensing of volatile organic compounds (VOCs) is critical to our perception of the environment around us,[1] monitoring of harmful emissions,[2] and healthcare analytics,[3] and so is required for a wide variety of current and future technologies.[4] Sensors based on metal–organic frameworks (MOFs) offer great potential, in particular towards selectivity, owing to their precisely defined pore structure and chemistry.[5–8] The modular nature of MOFs allows them to be tailored with highly specific host–guest interactions to adsorb small molecules with higher uptake and selectivity than conventional materials such as polymers, zeolites and porous carbons.[9,10] Luminescence and other optical transduction modes are most widely reported in the literature of MOF-based sensing;[11] however, for practical usage other modes that integrate more easily with existing electronics are more viable.[6,12] Whilst there have been a handful of encouraging reports of electronically-responsive MOFs,[13–17] MOFs can be ideal candidates for strain-induced chemical detection because of the deformations of coordination space within their crystal structures caused by host–guest interactions and their increased flexibility compared to conventional inorganic materials.[9,18–21] Micro-electro-mechanical systems (MEMS) sensors coated with thin films consisting of different MOFs such as ZIF-8 (ZIF, zeolitic imidazolate framework; ZIF-8 = Zn[2-methylimidazolate]$_2$) and HKUST-1 (HKUST, Hong Kong University of Science and Technology; HKUST-1, Cu$_3$[benzentricarboxylate]$_2$[H$_2$O]$_3$) have been shown to successfully respond to water, alcohols and other VOCs, with sensitivity limits that exceed other mass-sensitive sensors.[22,23] However, several challenges remain, including improving the ease of receptor layer preparation, selectivity, sensitivity and response time.[24,25] Often, parameters act against one another; *e.g.*, a thicker film may lead to increased sensitivity but at the cost of response time, owing to the time taken for analytes to diffuse through the MOF. In addition, the perceived necessity for well-adhered and defect-free, oriented thin films to effectively transmit analyte-induced strain to the sensor surface puts limits on the range of MOFs that can be used and introduces stringent, often laborious requirements to MEMS device fabrication.[5,24] On the other hand, a much wider range of MOFs can now be easily synthesized in colloidal or nanoparticular form.[26]

[a]School of Chemistry, University of Birmingham, Edgbaston, Birmingham, UK. E-mail: h.yeung@bham.ac.uk

[b]International Center for Young Scientists (ICYS), National Institute for Materials Science (NIMS), Tsukuba, Japan. E-mail: SHIBA.Kota@nims.go.jp

[c]Center for Functional Sensor & Actuator (CFSN), Research Center for Functional Materials, National Institute for Materials Science (NIMS), Tsukuba, Japan

[d]Materials Science and Engineering, Graduate School of Pure and Applied Science, University of Tsukuba, Tsukuba, Japan

[e]John A. Paulson School of Engineering and Applied Sciences, Harvard University, Cambridge, Massachusetts, USA

† Electronic supplementary information (ESI) available: Details of synthesis, materials characterisation, sensing experiments, finite element analysis (FEA) and statistical analysis. See DOI: 10.1039/d0ta07248f

‡ Previous address: Inorganic Chemistry Laboratory, University of Oxford, South Parks Road, Oxford, UK.

Nanoparticles (NPs) have been shown to be effective and simple to deposit *via* spray coating as receptor layer materials in MEMS sensors,[27–29] and size reduction has been shown to improve the mechanical stability of multilayer NP coatings.[30] Therefore, the integration of MOF NPs into MEMS devices would open up development of practical MOF-based sensors beyond those that form oriented thin films or are electronically conductive and lead to a new class of robust, selective receptor materials.

The membrane-type surface stress sensor (MSS) consists of a Si-based membrane suspended by four piezoresistive beams, composing a full Wheatstone bridge.[31] This architecture generates potential difference upon changes to the strain state of the membrane, with approximately 100 times greater sensitivity than conventional piezoresistive microcantilevers, and can be extended to multiple sensor arrays.[32] To induce strain on the membrane, a receptor layer bound to the membrane must undergo strain in response to an analyte. Modelling has predicted that receptor layer materials with higher Young's moduli tend to give better signals.[31,33]

Amongst a wide range of MOF NPs available, ZIFs exhibit mechanical properties somewhat intermediate within the MOF class of materials: they are stiffer than so-called "breathing" MOFs such as MIL-53 and pillared-layer MOFs, but still exhibit measurable flexibility in their crystal structure upon gas uptake.[34–37] Encouragingly for their potential sensing performance, it has been shown that particle size reduction to the nanoscale can result in rather linear gas adsorption isotherms,[38] and improved mechanical properties.[39] In addition, gas diffusion coefficients of bulk MOFs are often several orders of magnitude lower than that in air;[40,41] therefore, it could be reasonably expected that the meso- and macro-pores within a superstructure of MOF NPs will act as channels for analytes to rapidly diffuse through the whole receptor layer. Indeed, it has been shown using environmental ellipsometry that alcohol adsorption in thin films composed of ZIF-8 NPs takes just 20 s.[42] However, prior to this work it remained to be seen whether receptor layers built from MOF NPs would be able to induce sufficient strain in the MEMS sensors, in order to realize effective VOC sensing.

We herein report for the first time the fabrication and performance of a new MOF–MSS sensor based on NPs of the canonical ZIF family of MOFs (Fig. 1).[43] We first demonstrate the facile sensor fabrication using ZIF-8, which exhibits hydrophobic pores with the **sod** network topology.[43] We observe selectivity in its range of responses to 26 VOCs, with rapid response times of 1–30 s and ppm level sensitivity, and show that the sensor response is consistent with a mechanism of adsorbate-induced strain in the ZIF crystal lattice. Exploiting the versatility of the MSS architecture and the diversity of available MOF NPs, we use spray-coating to fabricate a 2 × 2 array of ZIF-8, ZIF-7 (Zn(benzimidazole)$_2$, **sod**), ZIF-65-Zn (Zn(2-nitroimidazole)$_2$, **sod**) and ZIF-71 (Zn(4,5-dichloroimidazole)$_2$, **rho**). The chemical diversity of these MOFs manifests itself in a wide range of sensing profiles, which enable clear discrimination between a range of different VOC classes and individual gases *via* principal component analysis.

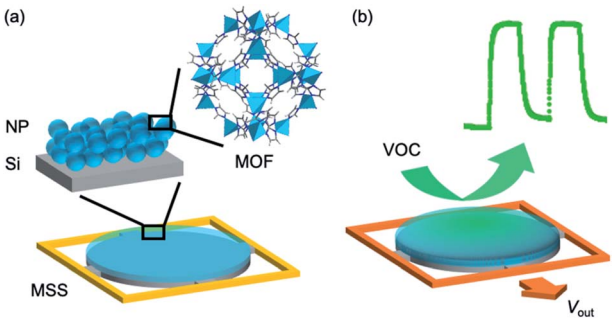

Fig. 1 Schematics of the novel MOF–MSS construction (a) and strain-based sensing concept (b). MOF nanoparticles (NP) are deposited directly on the Si surface of the MSS device. Adsorption of volatile organic compounds (VOC) results in strain in the MOF receptor layer, which is detected as a change in electronic output (V_{out}).

Materials and methods

Synthesis and characterisation

All chemicals are purchased from Tokyo Chemical Industry Co. Ltd, Sigma-Aldrich Co., Wako Pure Chemical Industries, Ltd, Kanto Chemical Co. Ltd and Nacalai Tesque, Inc. ZIF-8 NPs were synthesized following a literature protocol,[44] washed thrice in methanol to remove residual byproducts and resuspended in alcohol. ZIF-7, ZIF-65-Zn and ZIF-71 NPs were synthesized following similar literature routes (see ESI Section S1 for full details†).[45,46] Chemical composition, particle size and phase purity of bulk samples were confirmed by powder X-ray diffraction (XRD), Fourier transform-infrared (FT-IR), scanning electron microscopy (SEM), dynamic light scattering (DLS), zeta potential, Brunauer–Emmett–Teller (BET) surface area and thermogravimetric analysis (TGA) before and after activation under similar conditions used for sensor preparation (see ESI Section S2–S7†). Nitrogen gas sorption isotherms (ESI Section S6†) indicate significant mesoporosity and/or macroporosity in addition to the expected MOF microporosity, in line with previous reports.[44–46]

Sensor preparation

Materials were deposited directly onto the MSS membrane without any adhesive layer. For selectivity and VOC discrimination experiments, four methanolic suspensions of different ZIF NPs were deposited onto an MSS membrane array by spray coating 30 layers; a stage on which the MSS chip was mounted was held at 100 °C to rapidly evaporate the carrier solvent, and promote sintering and adhesion of the NPs to the surface. For investigation of sensitivity and response time, a ZIF-8 NP suspension was deposited on a single MSS membrane by inkjet deposition; an inkjet spotter (LaboJet-500SP) with a nozzle (IJHBS-300), which were purchased from the MICROJET Corporation, were utilized. The ZIF-8 NP suspension was loaded into the inkjet module, and up to 2500 sequential droplet depositions were performed. The inkjet stage was heated at 80 °C to control evaporation.

Sensing

Selectivity tests using the spray-coated ZIF-8-MSS were performed under ambient temperature using the saturated

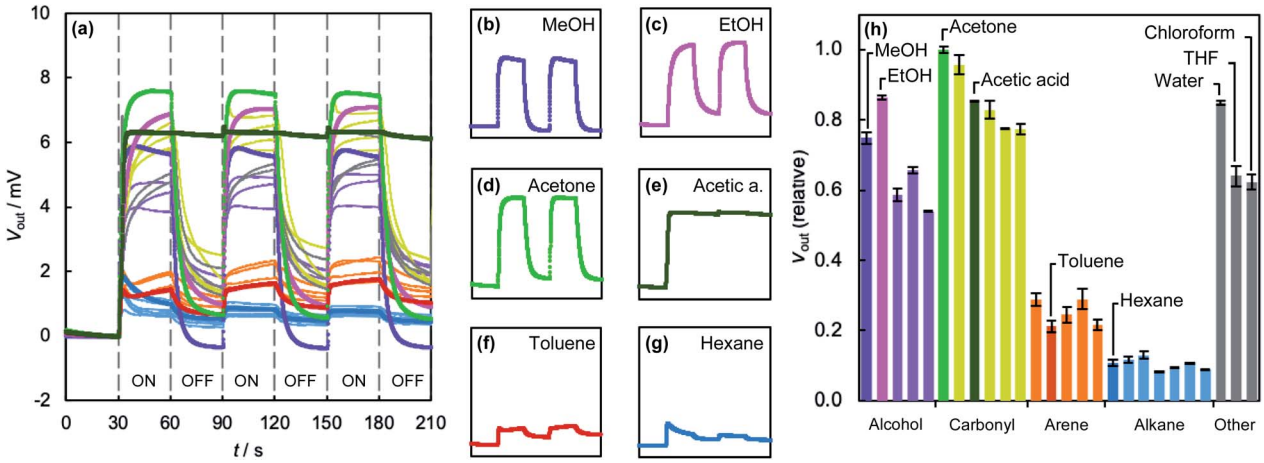

Fig. 2 Responses of the ZIF-8-MSS to saturated vapours at ambient temperature: (a) first three ON–OFF cycles for 26 VOCs, coloured according to class (alcohols – purple, carbonyls – green, arenes – orange, alkanes – blue, other – grey); representative response profiles (0–150 s) for methanol (170 000 ppm), ethanol (86 000 ppm), acetone (300 000 ppm), acetic acid (11 000 ppm), toluene (38 000 ppm) and hexane (190 000 ppm), are shown in, are shown in (b–g) respectively. (h) Relative mean response magnitudes calculated from three measurements for each gas; error bars represent two standard deviations. Colours correspond to those used in (a).

vapours of 26 VOCs, including those a range of alcohols, carbonyls, arenes and alkanes (see ESI Section S8 for details,† including absolute concentrations of saturated vapours). Gases were introduced to the sensor for 30 s *via* a custom-built setup and purged with nitrogen gas for 30 s. Four injection–purge (ON–OFF) cycles were performed for each gas and data were recorded at a sampling rate of 20 Hz by applying a bridge voltage of −0.5 V to the Wheatstone bridge. Discrimination tests for the VOCs using the 2 × 2 MOF–MSS array were performed in an identical manner. Sensitivity and response time were investigated using the inkjet-deposited ZIF-8-MSS for 12 VOCs under conditions of constant temperature and humidity using a separate setup (see ESI Section S9†). Gases were diluted to 2%, 5% and 10% of their saturated vapour concentrations and humidified at 0%, 10%, 40%, and 70% relative humidity (RH) prior to injection. Ten injection (10 s) – purge (10 s) cycles were performed for each measurement. Limits of detection were determined from the mean reversible response of cycles 2–4, divided by the electrical noise inherent in the MSS device (approximately 1 μV [31]) to give the signal-to-noise ratio. The effective limit of detection was then estimated by dividing the concentration of analyte present by the signal-to-noise ratio.

Principal component analysis (PCA)

The responses of the 2 × 2 MOF–MSS array were analysed following the methodology of Shiba *et al.* (see ESI Section S10†).[28] Briefly, the features of each response profile were decomposed into four parameters, defined as the rise rate, plateau rate, recovery rate and response magnitude. Parameters from the latter three of four cycles were used as inputs for PCA using Origin software, which determined the projection weights for a set of orthogonal principal components to maximise the total response variance.

Results and discussion

MOF–MSS sensor concept

We fabricated a MOF–MSS by spray-coating ZIF-8 NPs directly onto one of the membranes of the MSS array. Its response to the saturated vapour of 26 VOCs is shown in Fig. 2a (for details see ESI Section S11†). All gases were found to elicit a measurable response within seconds, including a range of alcohols, carbonyls, arenes, and alkanes. The irreversible signal—which we attribute to residual molecules that remain in the MOF pores on the timescale of these experiments—apparent in the first

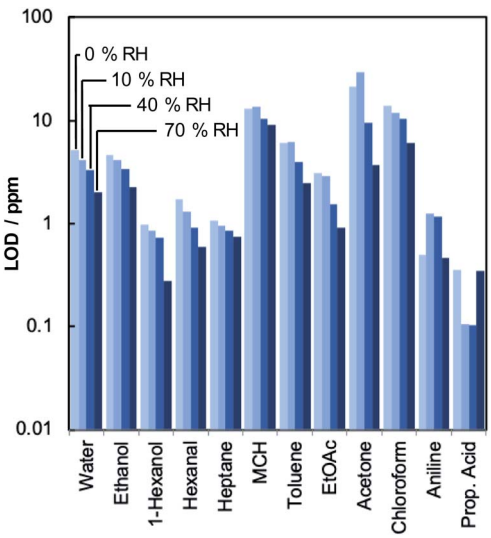

Fig. 3 Limit of detection (LOD) of a 2100 droplet nanoparticle ZIF-8-MSS sensor fabricated by inkjet deposition towards various analytes determined at 25 °C and humidity levels from 0% RH (light blue) to 70% RH (dark blue). MCH = methylcyclohexane; EtOAc = ethyl acetate; prop.acid = propionic acid.

cycle for most gases is largely absent from the second cycle onwards. Whilst these irreversible signals in the first cycle can be also caused by the enhanced concentration of VOC vapours in the head space of the vial prior to the measurements, they are not included in the following analyses.

Different classes of VOCs give rise to quite distinct response profiles. Water and alcohols, such as methanol (Fig. 2b) and ethanol (Fig. 2c) give amongst the highest output voltages and profiles that typically reach saturation within 30 s. Molecules with carbonyl functionality, such as ketones, esters and amides, including acetone (Fig. 2d), as well as chloroform and tetrahydrofuran also give large responses. The response of acetic acid (Fig. 2e) is unusual amongst the VOCs studied in that it is almost entirely irreversible on these timescales. We expect that this is due to the known instability of ZIFs in acidic conditions, which may degrade the receptor layer. Aromatic compounds, such as toluene (Fig. 2f), elicit intermediate responses that typically do not reach saturation within 30 s, whilst linear alkanes, including hexane (Fig. 2g), give rise to small responses that rapidly reach saturation and then decrease. We attribute the different saturation rates to the different diffusivities of these class of VOCs in ZIF-8; larger molecules will generally pass through the structure more slowly. We also note that the responses of the ZIF-8-based MSS do not necessarily correlate with previously reported[42] isotherms. Clearly, the response is a complex function of many factors, including host–guest interactions, diffusion through the receptor layer, mechanical properties and analyte-induced framework distortion. These factors are influenced by the structure of the MOF receptor layers on different levels, including composition, network topology, porosity (both within and between NPs), and particle–particle and particle-MSS interactions.

Optimisation of response magnitude and time

In order to determine the detection limits of the ZIF-8-MSS, the response magnitude and time were first optimized by investigating the effect of receptor layer volume (see ESI Section S12†). Devices were fabricated by inkjet deposition between 100 and 2500 droplets of a ZIF-8 NP suspension onto the MSS membrane. A device fabricated from 2100 inkjet droplets exhibited the best compromise between high output voltages and fast response times for selected gases from the five VOC classes investigated previously (methanol–alcohol, acetone–carbonyl, toluene–arene, heptane–alkane and water–other). Notably, for most receptor layer volumes, the response times for methanol, acetone and heptane were found to be less than 5 s, whilst for toluene and water they were consistently below 30 s. The device deposited with 2100 droplets was therefore chosen for the subsequent investigation of detection limits.

Detection limits

The sensitivity of the 2100-droplet ZIF-8-MSS was determined for 12 VOCs under variable humidity at 25 °C (Fig. 3). The sensor response typically decreased as the gases were diluted from 10% to 5% and then 2% saturated vapour. To calculate the limit of detection (LOD), the VOC concentration corresponding to 2% saturated vapour was multiplied by the ratio of 1 μV (the noise inherent to the MSS architecture; the experimental noise level can be higher depending on the measurement conditions)[31,32] and the average output voltage of three ON–OFF cycles. The sensor exhibited LODs for most gases well below 10 ppm and sub-ppm LODs to some, including 1-hexanol and *n*-heptane. Interestingly, sensitivity appears to improve with increasing humidity in some cases, suggesting that cooperative analyte–water interactions may be beneficial to the sensing mechanism. Increasing temperature typically results in reduced output. This is most likely because the receptor layer becomes softer[29] and the adsorption capacity of the MOF decreases.[47] It should be also noted that longer exposure to the vapors than the current cycles can yield even higher signal levels than the presented results, especially for the gas species with low concentrations. Such trends can be observed in some response signals that are not saturated in the current cycles. Accordingly, the detection limits depend also on the measurement conditions as the saturated signal levels are determined by the partial pressure of each gas in the case of chemical gas sensors based on the gas–solid equilibrium, including the present MOF–MSS as well as common chemoresistive sensors.[48,49]

Sensing mechanism

The MOF–MSS response was shown to be consistent with a mechanism of adsorbate-induced strain in the MOF receptor layer using Finite Element Analysis (FEA). The response is linear with respect to strain and depends on the Young's modulus, E_f, and, to a lesser extent, on the Poisson's ratio, ν_f, of the MOF receptor layer (see ESI Section S13†). It increases with receptor layer thickness up to a threshold value before decreasing at greater thickness. The thickness at which the response is maximised decreases as E_f and ν_f increase. Using representative values for E_f[39,50] and ν_f[51] of ZIF-8, the highest responses are calculated for receptor layer thicknesses between 8 μm and 10 μm. This range agrees favourably with the thickness calculated for the optimised 2100-droplet ZIF-8-MSS, which is 10.4 μm (see ESI Section S14†). FEA further indicates that it takes a strain of 1×10^{-4} to 2×10^{-4} in a ZIF-8-MSS with such a thickness to generate the range of observed responses, *i.e.*, 1–10 mV (Fig. S31a†). For example, methanol induces an output voltage of 10 mV in the 2100-droplet sensor (Fig. S28†), whilst the response of the spray-coated sensor to 1-butanol is around 5 mV (Fig. S34†). This is broadly consistent with previous analysis by powder XRD, which shows that full adsorption of 1-butanol induces a strain of 1.8×10^{-3} in the lattice parameter of ZIF-8.[52] Such a lattice strain is just an order of magnitude greater than the calculated strain in the ZIF-8 receptor layer overall. We attribute this difference to inhomogeneous coverage and imperfect interparticle and particle-surface adhesion, which are important to strain transduction in the sensor device and remain to be optimized in future work.

Multichannel array sensing

Despite reasonable selectivity that differentiates somewhat between VOCs, cross-sensitivity means that ZIF-8 is unable to

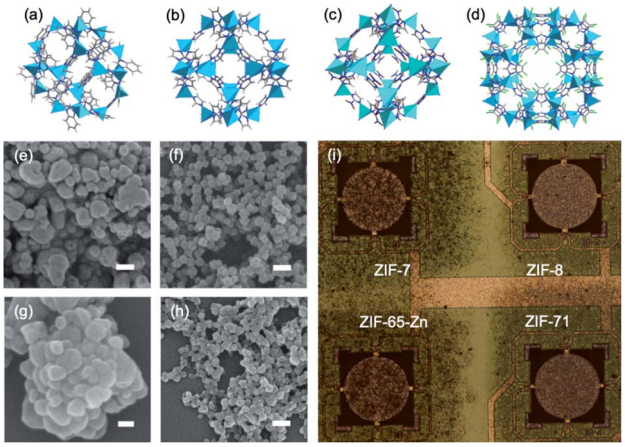

Fig. 4 Crystal structures of (a) ZIF-7, (b) ZIF-8, (c) ZIF-65–Zn and (d) ZIF-71. ZnN_4 tetrahedra are shown in blue; C, H, N, O and Cl atoms are shown in grey, white, blue, red and green, respectively. Methyl H atoms are not shown for clarity. Sample morphologies and device appearance of the 2 × 2 MOF–MSS array: (e–h) SEM images of representative NPs of ZIF-7, ZIF-8, ZIF-65–Zn and ZIF-71, respectively (scale bars = 200 nm); (i) optical micrograph of the MSS array spray-coated with (clockwise from top left) ZIF-7, ZIF-8, ZIF-71 and ZIF-65. Each membrane is 300 μm in diameter.

Table 1 Compositions, nets and pore aperture diameters (d_a), and pore diameters (d_p) of four ZIFs used in the 2 × 2 MOF–MSS array

MOF	Composition	Net	d_a/Å	d_p/Å
ZIF-7	$Zn(benzimidazole)_2$	**sod**	~3	4.3
ZIF-8	$Zn(2\text{-methylimidazole})_2$	**sod**	3.0	11.6
ZIF-65–Zn	$Zn(2\text{-nitroimidazole})_2$	**sod**	3.2	10.4
ZIF-71	$Zn(4,5\text{-dichloroimidazole})_2$	**rho**	4.2	16.5

unambiguously discriminate between multiple analytes. We adopted an multichannel array approach previously demonstrated for chemoresistive carbon nanotubes[53] and 2-D MOFs,[14] and exploited the versatility of the MOF–MSS concept to spray-coat a 2 × 2 array of MSS channels[31,32] with NPs of four ZIFs, ZIF-8,[54] ZIF-7,[45] ZIF-65–Zn and ZIF-71 [46] (Fig. 4). These particular MOFs were chosen because of their variety in composition, network topology, pore aperture, and diameter (Table 1); which may be expected to affect the adsorption of gases according to size, shape and/or functionality in different ways, thus leading to a diversity of responses and thus improved VOC discrimination.

Simultaneous sensing experiments using the MOF–MSS array reveal a wide variety of responses of the four ZIFs to 26 VOCs (Fig. 2h and 5; see also ESI Section S15†). The relative responses of the **sod** structures ZIF-7, ZIF-8 and ZIF-65 are qualitatively similar, reflecting the similarity in their network topologies and pore apertures. However, certain differences are apparent in, for example, response magnitudes (*e.g.*, acetic acid) or the relative responses of related compounds (*e.g.*, methanol *vs.* ethanol; acetic acid *vs.* acetone). Like in ZIF-8, arenes and linear alkanes elicit medium and low responses, respectively, in ZIF-7 and ZIF-65-Zn. It is particularly interesting that the responses of ZIF-65–Zn to both alkanes and arenes tend to decrease as molecular size increases. Its pore aperture is slightly bigger than the other **sod** analogues; perhaps this allows for more linear discrimination between compounds. The relative responses of ZIF-71 are qualitatively different to its **sod** analogues. Arenes and alkanes elicit higher responses, whilst methanol and ethanol give rise to lower responses. In this case, the response to alcohols appears to increase with increasing size of the molecules. ZIF-71 also gives a more uniform response across all VOCs. We tentatively attribute this to the openness of the **rho** net, which increases the reversibility of gas sorption compared to the other ZIFs, all of which exhibit the denser **sod** net. The relative decrease in response to short chain alcohols, such as methanol and ethanol, may be due to the hydrophobic nature of the dichloroimidazolate linker.

Statistical analysis

Further investigation of the multichannel data by principal component analysis (PCA) reveals that the 2 × 2 MOF–MSS array

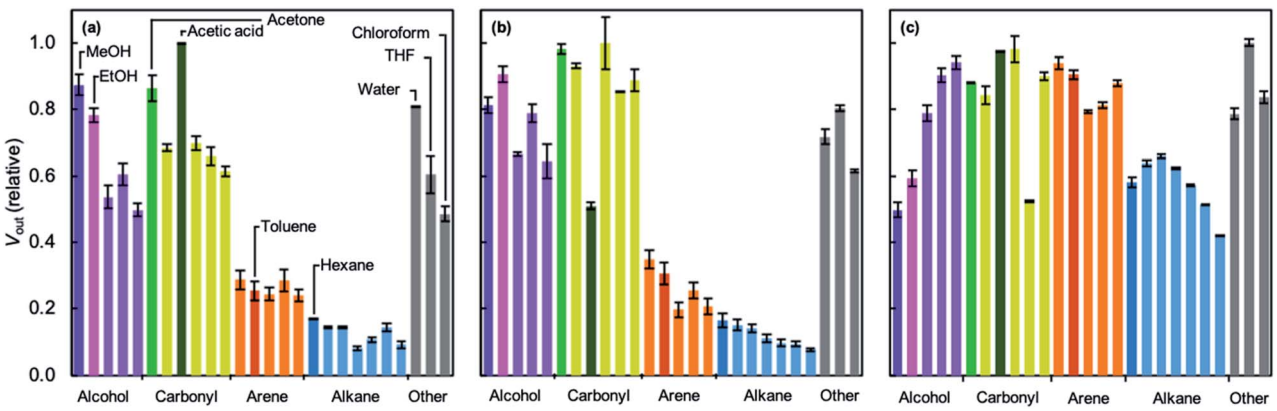

Fig. 5 Response of MOF–MSS array sensor membranes spray-coated with (a) ZIF-7, (b) ZIF-65–Zn, and (c) ZIF-71. Relative mean response magnitudes are calculated from three measurements for each gas; error bars represent two standard deviations. Colours correspond to those used in Fig. 2.

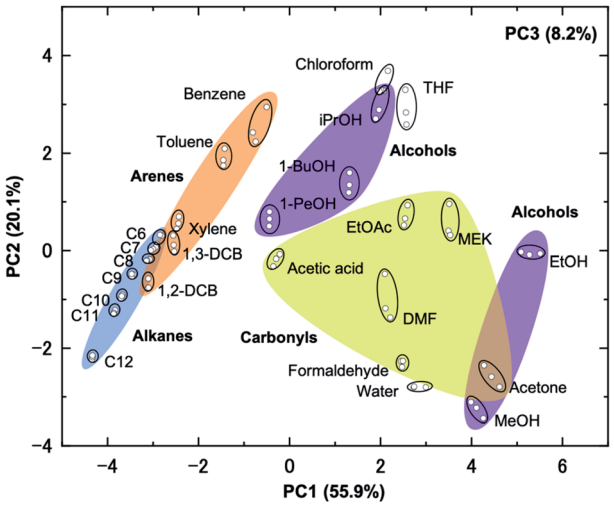

Fig. 6 Principal component analysis of response profile data from the 2 × 2 MSS array of ZIF NPs, using 26 VOCs.

is able to group VOCs by chemical class and even discriminate between individual gases. PCA is an unsupervised method of classifying multi-sensor data, which reduces the dimensionality of the dataset by representing the sensor contributions as linear combinations of the original variables in typically, two or three principal components (PCs).[55] Noting that the MOF–MSS response profiles contain a wealth of information beyond the simple magnitudes of response, we extracted parameters to describe the reversible response, uptake rate, plateau gradient and recovery rate of each ZIF in the 2× 2 array as input data for PCA (see ESI Section S10†).[28,32] It was found that the four classes of VOCs could successfully be discriminated using just two PCs, with only small ambiguities in the case of overlaps between alcohols and carbonyls (*e.g.*, acetone), and arenes and alkanes (*e.g.*, shorter chain alkanes and dichlorobenzenes) (Fig. 6). Interestingly, alcohols appear to be subdivided into two groups, one with the smallest molecules (methanol and ethanol) and the other with larger molecules. The weightings of PC1 and PC2 were 55.9% and 20.1%, respectively, and together they describe 75.0% of the total variance. A third principal component (PC3 = 8.2%) was found to improve the description to 83.2% and, when viewed with PC1, suggests a much closer grouping of the alcohols (see ESI Section S16†). Within each class, the repeatability of our measurements is apparent in the ability to clearly discriminate between different VOCs. This is an advantage for VOC identification applications, for which there is prior knowledge of a given analyte's response. For example, methanol and ethanol are clearly distinguishable from each other, as are methylethylketone and acetone, both pairs of which differ by just one CH_2 group. Alkanes and aromatic molecules follow clear trends with molecular size, which could be useful in monitoring separation processes.

Conclusions

We have demonstrated for the first time that MOF NPs as a receptor layer on the MSS platform can be highly effective for strain-based chemical sensing. Response times of 1–30 s represent an order of magnitude improvement over existing MOF strain-based sensors (see ESI Section S17†). Sub-ppm sensitivity towards a range of VOCs again represents an improvement in strain-based sensing using MOFs, bringing it on par with hard-to-fabricate photonic crystal thin films,[56] interdigitated electrode devices[57–59] and colorimetric sensors,[60] the latter of which was limited in analyte scope to water. Importantly, we have demonstrated that, in principle, any MOF that can be made in NP form[26] can now be employed in strain-based sensing, which allows for an enormous diversity of chemistries and VOC selectivities. We constructed a 2 × 2 MSS array using four ZIFs, which have different responses to a range of VOCs and, when their combined responses are subjected to PCA, are able to successfully group the VOCs by class and discriminate between them. Whilst the performance of the reported MOF–MSS is extremely promising, other aspects, such as particle–particle adhesion, particle-surface adhesion and mesoporosity, remain to be optimized in further work. These and many other factors may affect the sensing performance. Therefore, fundamental studies in areas such as MOF–guest interaction energetics, diffusion and flexibility will undoubtedly aid progress in this regard.

Conflicts of interest

The authors hold a patent related to the described work (JP 06544744, US 10564082).

Acknowledgements

We thank the World Premier International Research Center Initiative on Materials Nanoarchitectonics (WPI-MANA) from MEXT, Japan for financial and technical support. This work was also supported by JSPS KAKENHI Grant Number JP19KK0141, MEXT, Japan; a Grant-in-Aid for Scientific Research (A), 18H04168, MEXT, Japan; the Public/Private R&D Investment Strategic Expansion Program (PRISM), Cabinet Office, Japan; the Center for Functional Sensor and Actuator (CFSN). HHMY acknowledges support from the Glasstone Bequest for financial support through the provision of a Glasstone Fellowship and the University of Birmingham for startup funds. We thank Mr Makito Nakatsu for performing BET measurements and Ms. Yuko Kameyama, Ms Keiko Koda, Ms Eri Sakon and Ms Ikumi Nakakubo (WPI-MANA, NIMS) for coating the ZIFs and collecting all the sensing data. This work was born out of many fruitful discussions at the International Center for Young Scientists (ICYS) at NIMS.

References

1 I. Chou, T. Chouard, J. E. Spiro and L. Anson, *Nature*, 2006, **444**, 287.
2 D. J. Wales, J. Grand, V. P. Ting, R. D. Burke, K. J. Edler, C. R. Bowen, S. Mintova and A. D. Burrows, *Chem. Soc. Rev.*, 2015, **44**, 4290–4321.
3 B. Buszewski, M. Kęsy, T. Ligor and A. Amann, *Biomed. Chromatogr.*, 2007, **21**, 553–566.

4 F.-G. Bănică, *Chemical Sensors and Biosensors*, Wiley, 2012.
5 L. E. Kreno, K. Leong, O. K. Farha, M. Allendorf, R. P. Van Duyne and J. T. Hupp, *Chem. Rev.*, 2012, **112**, 1105–1125.
6 I. Stassen, N. Burtch, A. Talin, P. Falcaro, M. Allendorf and R. Ameloot, *Chem. Soc. Rev.*, 2017, **46**, 3185–3241.
7 Y. Li, A. S. Xiao, B. Zou, H. X. Zhang, K. Le Yan and Y. Lin, *Polyhedron*, 2018, **154**, 83–97.
8 P. Canepa, K. Tan, Y. Du, H. Lu, Y. J. Chabal and T. Thonhauser, *J. Mater. Chem. A*, 2015, **3**, 986–995.
9 S. Horike, S. Shimomura and S. Kitagawa, *Nat. Chem.*, 2009, **1**, 695–704.
10 H. Furukawa, K. E. Cordova, M. O'Keeffe and O. M. Yaghi, *Science*, 2013, **341**, 1230444.
11 J. Dong, D. Zhao, Y. Lu and W. Y. Sun, *J. Mater. Chem. A*, 2019, **7**, 22744–22767.
12 M. D. Allendorf, A. Schwartzberg, V. Stavila and A. A. Talin, *Chemistry*, 2011, **17**, 11372–11388.
13 A. Chidambaram and K. C. Stylianou, *Inorg. Chem. Front.*, 2018, **5**, 979–998.
14 M. G. Campbell, S. F. Liu, T. M. Swager and M. Dincă, *J. Am. Chem. Soc.*, 2015, **137**, 13780–13783.
15 M. G. Campbell, D. Sheberla, S. F. Liu, T. M. Swager and M. Dincă, *Angew. Chem., Int. Ed.*, 2015, **54**, 4349–4352.
16 V. Chernikova, O. Yassine, O. Shekhah, M. Eddaoudi and K. N. Salama, *J. Mater. Chem. A*, 2018, **6**, 5550–5554.
17 N. A. Travlou, K. Singh, E. Rodríguez-Castellón and T. J. Bandosz, *J. Mater. Chem. A*, 2015, **3**, 11417–11429.
18 G. Ferey, *Z. Anorg. Allg. Chem*, 2012, **638**, 1897–1909.
19 A. Schneemann, V. Bon, I. Schwedler, I. Senkovska, S. Kaskel and R. A. Fischer, *Chem. Soc. Rev.*, 2014, **43**, 6062–6096.
20 S. Kitagawa and R. Matsuda, *Coord. Chem. Rev.*, 2007, **251**, 2490–2509.
21 S. Wannapaiboon, M. Tu, K. Sumida, K. Khaletskaya, S. Furukawa, S. Kitagawa and R. A. Fischer, *J. Mater. Chem. A*, 2015, **3**, 23385–23394.
22 M. D. Allendorf, R. J. T. Houk, L. Andruszkiewicz, A. A. Talin, J. Pikarsky, A. Choudhury, K. A. Gall and P. J. Hesketh, *J. Am. Chem. Soc.*, 2008, **130**, 14404–14405.
23 C. Yim, M. Lee, W. Kim, S. Lee, G.-H. Kim, K. T. Kim and S. Jeon, *Chem. Commun.*, 2015, **51**, 6168–6171.
24 D. Bradshaw, A. Garai and J. Huo, *Chem. Soc. Rev.*, 2012, **41**, 2344–2381.
25 A. Bétard and R. A. Fischer, *Chem. Rev.*, 2012, **112**, 1055–1083.
26 M. Sindoro, N. Yanai, A. Y. Jee and S. Granick, *Acc. Chem. Res.*, 2014, **47**, 459–469.
27 K. Shiba, T. Takei, G. Yoshikawa and M. Ogawa, *Nanoscale*, 2017, **9**, 16791–16799.
28 K. Shiba, R. Tamura, G. Imamura and G. Yoshikawa, *Sci. Rep.*, 2017, **7**, 3661.
29 K. Shiba, R. Tamura, T. Sugiyama, Y. Kameyama, K. Koda, E. Sakon, K. Minami, H. T. Ngo, G. Imamura, K. Tsuda and G. Yoshikawa, *ACS Sens.*, 2018, **3**, 1592–1600.
30 W. Heni, L. Vonna and H. Haidara, *Nano Lett.*, 2015, **15**, 442–449.
31 G. Yoshikawa, T. Akiyama, S. Gautsch, P. Vettiger and H. Rohrer, *Nano Lett.*, 2011, **11**, 1044–1048.
32 G. Yoshikawa, T. Akiyama, F. Loizeau, K. Shiba, S. Gautsch, T. Nakayama, P. Vettiger, N. F. de Rooij and M. Aono, *Sensors*, 2012, **12**, 15873–15887.
33 G. Yoshikawa, *Appl. Phys. Lett.*, 2011, **98**, 98–101.
34 S. A. Moggach, T. D. Bennett and A. K. Cheetham, *Angew. Chem., Int. Ed.*, 2009, **48**, 7087–7089.
35 P. Zhao, G. I. Lampronti, G. O. Lloyd, E. Suard and S. A. T. Redfern, *J. Mater. Chem. A*, 2014, **2**, 620–623.
36 J. Im, N. Yim, J. Kim, T. Vogt and Y. Lee, *J. Am. Chem. Soc.*, 2016, **138**, 11477–11480.
37 C. L. Hobday, T. D. Bennett, D. Fairen-Jimenez, A. J. Graham, C. A. Morrison, D. R. Allan, T. Düren and S. A. Moggach, *J. Am. Chem. Soc.*, 2018, **140**, 382–387.
38 C. Zhang, J. A. Gee, D. S. Sholl and R. P. Lively, *J. Phys. Chem. C*, 2014, **118**, 20727–20733.
39 T. Tian, J. Velazquez-Garcia, T. D. Bennett and D. Fairen-Jimenez, *J. Mater. Chem. A*, 2014, **3**, 2999–3005.
40 K. Eum, K. C. Jayachandrababu, F. Rashidi, K. Zhang, J. Leisen, S. Graham, R. P. Lively, R. R. Chance, D. S. Sholl, C. W. Jones and S. Nair, *J. Am. Chem. Soc.*, 2015, **137**, 4191–4197.
41 F. Rashidi, C. R. Blad, C. W. Jones and S. Nair, *AIChE J.*, 2016, **62**, 525–537.
42 A. Demessence, C. Boissière, D. Grosso, P. Horcajada, C. Serre, G. Férey, G. J. a. a. Soler-Illia and C. Sanchez, *J. Mater. Chem.*, 2010, **20**, 7676–7681.
43 K. S. Park, Z. Ni, A. P. Cote, J. Y. Choi, R. Huang, F. J. Uribe-Romo, H. K. Chae, M. O'Keeffe and O. M. Yaghi, *Proc. Natl. Acad. Sci. U. S. A.*, 2006, **103**, 10186–10191.
44 J. Cravillon, S. Münzer, S. J. Lohmeier, A. Feldhoff, K. Huber and M. Wiebcke, *Chem. Mater.*, 2009, **21**, 1410–1412.
45 Y. S. Li, F. Y. Liang, H. Bux, A. Feldhoff, W. S. Yang and J. Caro, *Angew. Chem., Int. Ed.*, 2010, **49**, 548–551.
46 M. Tu, C. Wiktor, C. Rösler and R. A. Fischer, *Chem. Commun.*, 2014, **50**, 13258–13260.
47 C. Y. Huang, M. Song, Z. Y. Gu, H. F. Wang and X. P. Yan, *Environ. Sci. Technol.*, 2011, **45**, 4490–4496.
48 B. J. Doleman, E. J. Severin and N. S. Lewis, *Proc. Natl. Acad. Sci. U. S. A.*, 1998, **95**, 5442–5447.
49 K. Minami, K. Shiba and G. Yoshikawa, *Anal. Methods*, 2018, **10**, 3720–3726.
50 J. C. Tan, T. D. Bennett and A. K. Cheetham, *Proc. Natl. Acad. Sci. U. S. A.*, 2010, **107**, 9938–9943.
51 J. C. Tan, B. Civalleri, C. C. Lin, L. Valenzano, R. Galvelis, P. F. Chen, T. D. Bennett, C. Mellot-Draznieks, C. M. Zicovich-Wilson and A. K. Cheetham, *Phys. Rev. Lett.*, 2012, **108**, 1–6.
52 J. Cousin Saint Remi, T. Rémy, V. Van Hunskerken, S. Van de Perre, T. Duerinck, M. Maes, D. De Vos, E. Gobechiya, C. E. A. Kirschhock, G. V. Baron and J. F. M. Denayer, *ChemSusChem*, 2011, **4**, 1074–1077.
53 F. Wang and T. M. Swager, *J. Am. Chem. Soc.*, 2011, **133**, 11181–11193.
54 J. Cravillon, S. Münzer, S.-J. Lohmeier, A. Feldhoff, K. Huber and M. Wiebcke, *Chem. Mater.*, 2009, **21**, 1410–1412.
55 P. C. Jurs, G. A. Bakken and H. E. McClelland, *Chem. Rev.*, 2000, **100**, 2649–2678.

56 G. Lu, O. K. Farha, L. E. Kreno, P. M. Schoenecker, K. S. Walton, R. P. Van Duyne and J. T. Hupp, *Adv. Mater.*, 2011, **23**, 4449–4452.
57 H. Yuan, J. Tao, N. Li, A. Karmakar, C. Tang, H. Cai, S. J. Pennycook, N. Singh and D. Zhao, *Angew. Chem., Int. Ed.*, 2019, **58**, 14089–14094.
58 O. Yassine, O. Shekhah, A. H. Assen, Y. Belmabkhout, K. N. Salama and M. Eddaoudi, *Angew. Chem., Int. Ed.*, 2016, **55**, 15879–15883.
59 Z. Meng, A. Aykanat and K. A. Mirica, *J. Am. Chem. Soc.*, 2019, **141**, 2046–2053.
60 S. I. Ohira, Y. Miki, T. Matsuzaki, N. Nakamura, Y. Sato, Y. Hirose and K. Toda, *Anal. Chim. Acta*, 2015, **886**, 188–193.